Multi-resonant Microfabricated Inductors and Transformers

Joshua Phinney, Jeffrey H. Lang, and David J. Perreault
LABORATORY FOR ELECTROMAGNETIC AND ELECTRONIC SYSTEMS
MASSACHUSETTS INSTITUTE OF TECHNOLOGY, ROOM 10–171
CAMBRIDGE, MASSACHUSETTS 02139
EMAIL: jphinney@mit.edu

***Abstract*— This paper introduces (1) a family of multi-resonant passive components with harmonically related impedance nulls and maxima, (2) board- and wafer-scale construction techniques for such structures, and (3) circuit topologies that exploit the harmonically related impedance extrema they provide. A three-dimensional copper electroforming process has been developed which offers an integrated-circuit designer larger-valued, higher-Q power inductors than are achievable with traditional thin-film processing. Such magnetic structures, whether fabricated in printed-circuit form or electroformed on a wafer, can be tapped to produce integrated multi-resonant L-C networks. These networks can develop much larger impedance than the corresponding untapped structure, provide self-shielding, eliminate switches from symmetric converter topologies, and otherwise reduce switch stresses. As part of the broader treatment, a new soft-switched radio-frequency power converter is introduced that demonstrates the reduction in peak device stress and passive-component size achievable with multi-resonant components. Taken together, the construction techniques, networks, and converter topologies presented here extend the power levels and applications for which passive components can be manufactured in an integrated fashion, alongside semiconductor switches and converter controls.**

I. INTRODUCTION

ENERGY-PROCESSING circuitry — the power electronics necessary for electronic and electrical equipment of all types — notoriously resists miniaturization comparable to that of MEMS and microelectronic systems. The size of passive components largely accounts for the bulk of power electronics: such components must be large, typically too large for on-die manufacture, if they are to develop useful impedances with losses permitted by the efficiency and thermal requirements of a power converter. Power inductors and transformers, in particular, are challenging to miniaturize because of their poor performance when scaled down in size, and the difficulty of fabricating them with available planar processes. There is an evident demand for new technologies which enable power passive components to be batch-fabricated in an integrated fashion, or equivalently, which reduce the size of reactive components required for a given level of power-converter performance.

This paper describes new design and fabrication methods for micro-scale passive components and the converters that employ them. In Section II, we introduce a network structure with multiple harmonically related resonances, able to generate impedances — at select frequencies — that greatly exceed those achieved by conventional passives of comparable size. Aligned impedance nulls of such structures, likewise, can enforce half-wave symmetric waveforms at the network terminals, reducing switch stresses or altogether eliminating switches from double-ended converter topologies. We next describe, in Section III, how harmonic impedance characteristics can be developed by lumped transmission-line analogs, in particular by self-shielding, capacitively tapped toroids. Section IV outlines processes for constructing such structures at both the printed-circuit-board and integrated-circuit level. Here we detail a low-temperature, batch-fabrication scheme for electroforming toroids on the surface of wafers or other substrates. Section V describes some power-electronics applications of multi-resonant components. A new soft-switched RF inverter incorporating a multi-resonant inductor is introduced and experimentally demonstrated. By simultaneously extending the practical batch-fabricated sizes of passive components while reducing their requisite values, the techniques presented here will broaden the power levels and applications for which fully integrated power electronics are feasible.

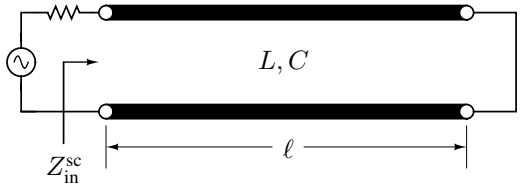

Fig. 1. **A uniform, lossless transmission line used to introduce the frequency relationships of impedance nulls and peaks.**

II. BACKGROUND AND MOTIVATION

The advantages of harmonically related impedance nulls and eigenvalues can be illustrated by considering the frequency relationships that arise in uniform, lossless transmission lines. Fig. 1a illustrates a line of length ℓ, short-circuited at the far end. If L and C are the distributed inductance and capacitance per unit length, the input impedance is a transcendental function with an infinite number of j-axis poles:

$$Z_{\text{in}}^{\text{sc}} = j\sqrt{\frac{L}{C}}\tan\omega\ell\sqrt{LC} \tag{1}$$

The zeros of $Z_{\text{in}}^{\text{sc}}$ are seen to lie $s = j\omega_\nu$, where

$$\omega_\nu = \frac{\nu\pi}{2\ell\sqrt{LC}} \quad \text{for } \nu = 0, 2, 4, ... \tag{2}$$

The admittance, likewise, is

$$Y_{\text{in}}^{\text{sc}} = -j\sqrt{\frac{C}{L}}\cot\omega\ell\sqrt{LC} \tag{3}$$

so that the poles of $Z_{\text{in}}^{\text{sc}}$ are described by Eqn. 2 for *odd integral* ν. By a similar development for an open-circuit termination,

0-7803-8399-0/04/$20.00 ©2004 IEEE.

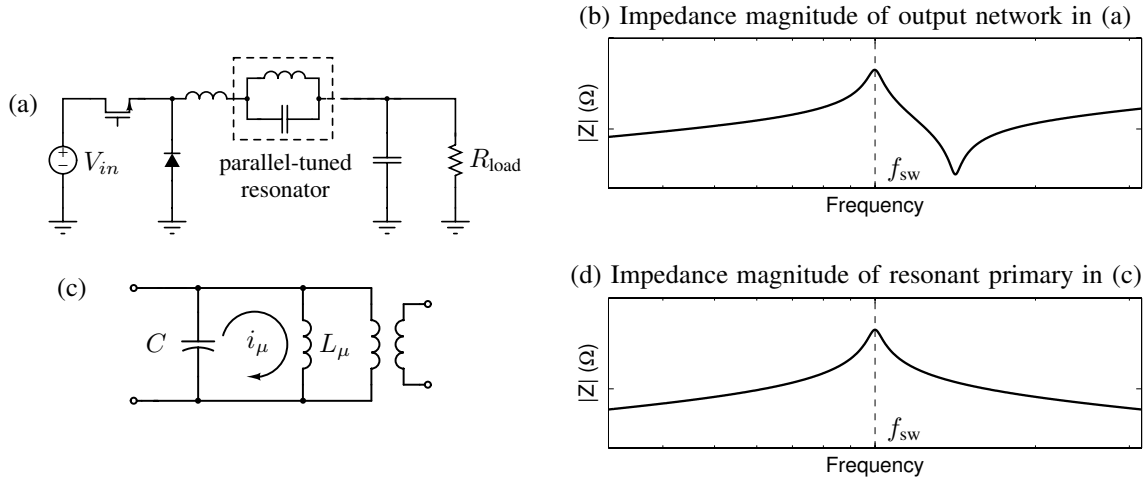

Fig. 2. **(a) Buck converter demonstrating the reduction in output-network component values by the introduction of a parallel-tuned resonance. As shown in (b), the output-network presents a high impedance at the converter switching frequency f_{sw}. The resonant transformer in (c) illustrates how magnetizing current i_μ can be supplied by the capacitance C, increasing the impedance (d) seen from the primary terminals at a discrete frequency.**

$Z_{\text{in}}^{\text{oc}}$ is maximum at DC and all even integral multiples of the first null frequency. In a converter whose switching frequency is aligned to the first impedance maximum of a transmission line, therefore, the open-circuit line presents high impedance at *all integral multiples* of the switching fundamental.

To understand the advantages of odd-harmonic and full-harmonic immitance maxima, consider the advantages of the single-resonant case. Resonant ripple filters with active tuning control [1], [2], [3], [4] use the immitance peaking of series- and parallel-tuned networks (e.g., Fig. 2a) to provide extra attenuation at discrete frequencies, reducing the requirements on accompanying low-pass networks. By requiring high immitance only at frequencies of interest (e.g., the switching fundamental), the size of passive components can be reduced three times or more [1], [2]. Increased impedance at a drive frequency, more specifically, makes feasible the use of components with manufacturing or cost advantages. The magnetizing inductance L_μ of air-core transformers and inductors, for instance, are typically too low for many practical power-conversion applications. A capacitor in parallel with a low L_μ (Fig. 2c) decreases the current supplied by the driving network — at a specific frequency — by ringing the magnetizing current i_μ from an internal mode of energy storage. Such single-resonant techniques have made practical printed-magnetic implementations of gate drives and isolated converters [5].

Multi-resonant extensions of networks like those in Fig. 2 can realize even greater size and performance advantages than their single-resonant counterparts. As will be explored in Section V, placing zeros and poles to develop large impedance differences at even and odd harmonics allows useful waveform symmetries to be imposed. These symmetries can be used to reduce device stresses, or even eliminate circuit components in some cases.

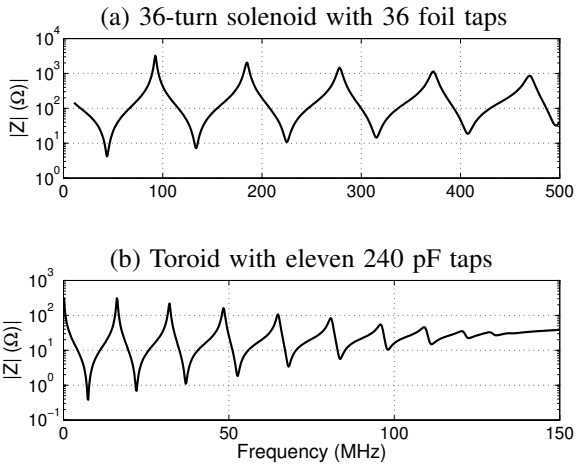

Fig. 3. **Iterated L-section filters demonstrating a near-harmonic alignment of impedance peaks and nulls: (a) impedance of a 36-turn PCB solenoid 0.3 in wide and 1.2 in long with mylar-foil capacitor taps (peaks at 2.000, 3.0007, 4.027, and 5.074 times the lowest peak frequency of 92.50 MHz). (b) impedance of the 0.75 in-diameter PCB toroid with 11 240 pF taps, shown in Fig 6. Impedance maxima are at 1.988, 3.000, 4.023, and 5.011 times the lowest peak frequency of 16.13 MHz; nulls are 2.950, 4.924, 7.024, and 9.074 times the first zero at 7.50 MHz. Both structures were constructed in a double-sided, 65 mil-thick FR-4 PCB.**

III. Design of Multi-resonant structures

A harmonic alignment of impedance peaks and nulls is readily approximated by a capacitively tapped inductor such as that in Fig. 4. The measured open-circuit impedances of two such tapped structures — a linear solenoid and a toroidal inductor built into the thickness of printed-circuit boards [1] — are plotted in Fig 3. Both structures demonstrate integral eigenvalue alignment within 1% of frequency up to the 5^{th} peak, and the toroid shows zero alignment within 2% of frequency up to

[1]For the case of rectangular winding cross-sections, self inductances of straight windings were computed using Niwa's rectangular current-sheet approximation, reported by Grover[6].

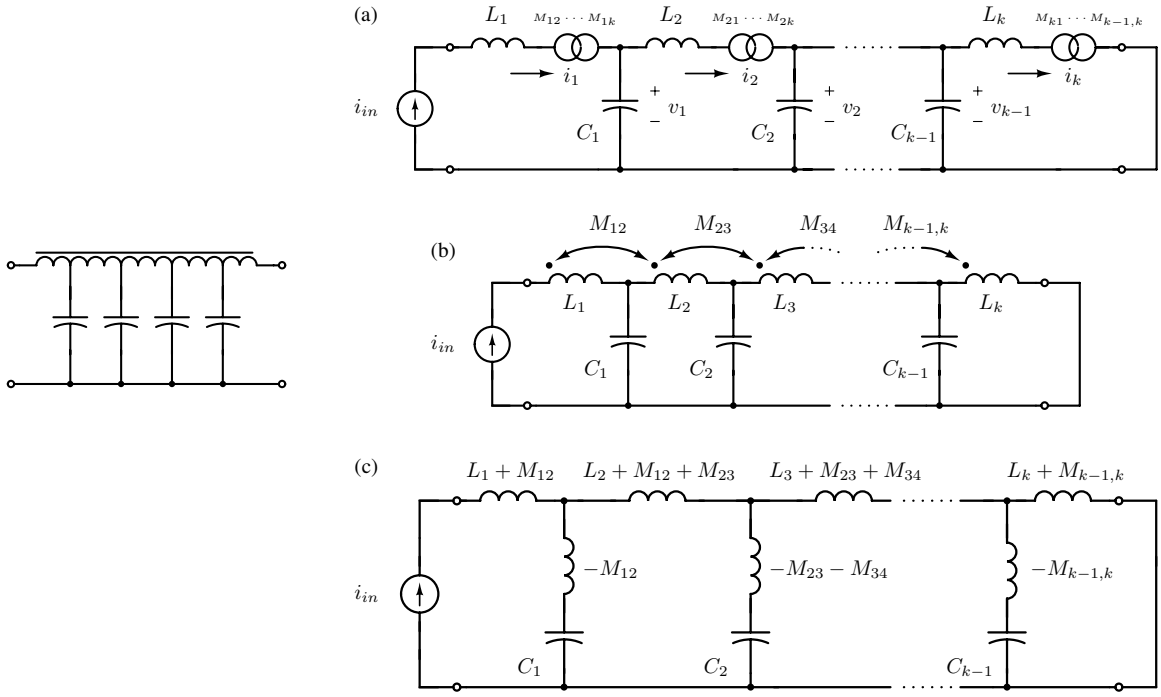

Fig. 4. **A tapped inductor, left, and the network models (a)-(c) used to predict its impedance**

TABLE I
POLE AND ZERO FREQUENCIES FOR THE IMPEDANCE PLOTS OF FIG. 3.

Structure	**Pole Frequency** (MHz)	**Zero Frequency** (MHz)
solenoid	92.50	43.75
	185.00	133.75
	278.13	225.00
	372.50	315.00
	469.38	407.50
toroid	16.13	7.50
	32.06	22.13
	48.38	22.13
	64.88	36.94
	80.81	52.69

the 5^{th} null. Consistent shifts in critical frequencies, e.g., low zero values with respect to the first peak, can be altered by the proper terminal impedance. Removing lead inductance in the impedance measurement, for instance, will move the zeros up in frequency while leaving the network eigenvalues nearly unaltered (see Appendix and Fig. 14). More detailed synthesis methods that use non-uniform L and C to place zeros and poles at precise frequencies are elaborated in the Appendix.

The approximately integral relationship of peaks and nulls noted above is not surprising: apart from mutual inductances (Fig. 4a), a tapped inductor resembles a lumped analog of a transmission line comprising iterated L- or T-sections. As discretization increases, one would expect the transmission-line impedance approximation to improve. Indeed, just as the inductance and capacitance *per unit length* determine all propagation and impedance characteristics of a line, so one would seem justified in adding — in the interest of a closer harmonic approximation — as many capacitive taps as possible to an inductor, while maintaining the same total capacitance and resonant frequencies. The mutual inductances, however, complicate this insight, effectively changing the electrical length of the lumped analog as it is tapped more densely. For the case of air-core inductors that are laterally thin with respect to the magnetic axis, however, the mutual inductances can be extremely useful.

In thin, air-core magnetic structures, mutual inductance terms apart from those between immediately adjacent sections of the tapped inductor are negligible. The section-to-section inductance matrix has a banded structure, as represented by the couplings of Fig. 4b. In such a case, a Δ-Y transformation for the coupled inductors introduces a *negative inductance* in the capacitive-tap branch, with a value equal to the sum of the mutual inductances for each inductor-section communicating with the tap. The number of taps on the overall inductor can be chosen such that this negative branch inductance approximately cancels the equivalent series inductance of the tap capacitors [7]. Inductance cancellation prevents the order of the overall structure from collapsing beyond the self-resonant frequency of the capacitors.

Building upon the derivation of lumped models for transmission lines presented in the Appendix, we can express the first non-zero peaks and nulls of iterated networks in terms of their total inductance L_{tot} and total capacitance C_{tot}. For alignment with some switching frequency f_{sw}, we simply choose a L_{tot} and C_{tot} to have the correct product (see below), while setting the ratio $L_{\text{tot}}/C_{\text{tot}}$ from manufacturing or characteristic-impedance considerations. A design with larger inductances

and smaller tap-capacitance, for instance, will ring up to higher impedances for the same Q, with capacitor-plate areas that may be less expensive to realize in a multi-layer PCB (see Sec. IV).

The relationship of L_{tot} and C_{tot} to the first non-zero peaks and nulls are given by L and C values for simulating networks, i.e., for the second-order series- or parallel-tuned networks which approximate the peak or null impedance in its vicinity. These networks are parameterized by the index of the corresponding critical frequency, i.e., the indexing of all interleaved poles and zeros which beginning with 0 for the DC pole or zero. For impedance zeros in a short-circuited line, the series-tuned network is given by.

$$L_\nu = \frac{L_{\text{tot}}}{2} \qquad C_\nu = \frac{8C_{\text{tot}}}{\nu^2\pi^2}$$

The first nonzero null has an index $\nu = 2$ (i.e., $\nu = 0$ for the DC zero, $\nu = 1$ for the first peak). If we wish to align the zeros of a short-circuited transmission-line analog to even harmonics of a switching frequency, we would choose L_2 and C_2 to resonate at $2f_{\text{sw}}$:

$$2f_{\text{sw}} = \frac{1}{2\pi}\left[\sqrt{\frac{L_{\text{tot}}}{2}\cdot\frac{2C_{\text{tot}}}{\pi^2}}\right]^{-1} = \frac{1}{2\sqrt{L_{\text{tot}}C_{\text{tot}}}} \qquad (4)$$

Alternately, we might wish to align the first non-zero eigenvalue of an open-circuited network to a switching frequency. The impedance peaks in this case are described by parallel-tuned simulating networks with values:

$$L_\nu = \frac{8L_{\text{tot}}}{\nu^2\pi^2} \qquad C_\nu = \frac{C_{\text{tot}}}{2}$$

The mode of interest again has an index $\nu = 2$, so our alignment condition expressed in terms of total capacitance and inductance becomes:

$$2\pi f_{\text{sw}} = \left[\sqrt{\frac{2L_{\text{tot}}}{\pi^2}\cdot\frac{C_{\text{tot}}}{2}}\right]^{-1} = \frac{\pi}{\sqrt{L_{\text{tot}}C_{\text{tot}}}} \qquad (5)$$

Relationships such as Eqns. 4 and 5 — in terms of L_{tot} and C_{tot} — are convenient means of comparing a transmission-line analog to alternate filters and power stages. A designer can easily compute, for instance, the knee frequency of a second-order filter comprising the total line capacitance and inductance, and compare the roll-off of such a filter to the attenuation provided by a practical resonance.

Though the poles and zeros of multi-resonant structures, particularly those in the so-called Cauer form, depend on the component values in each section, relative frequency alignment in the overall structure can still be good because of tight *ratiometric* control. Mask-based fabrication techniques (see Sec. IV) ensure low relative mismatch among capacitances, for instance, or among the loop area of turns. For applications in which poor absolute tolerance is unacceptable, a converter's switching frequency can be placed under closed-loop control to ensure that resonant attenuation at multiple harmonics is always maintained [1], [2], [3], [4].

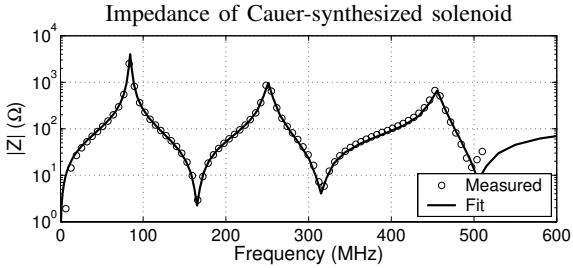

Fig. 9. **Measured impedance magnitude of the PCB solenoid shown in Fig. 6b, plotted with the magnitude of a 12^{th}-order fit used in simulations.**

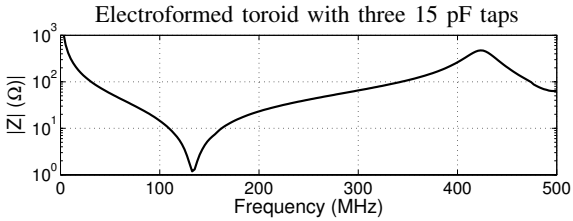

Fig. 10. **Measured impedance magnitude of a wafer-level solenoid. The structure had a 10 MHz Q of 9.8 and an inductance of 48 nH at the same frequency.**

IV. Fabrication

Tapped toroids and solenoids were built in two forms: embedded in a four-layer printed-circuit board (PCB), and electroplated on pyrex substrates with mask-based imaging of deposited layers.

A. Printed-Circuit Board Structures

A cross-section of a PCB device is shown in Fig. 5a, alongside mask views of inner and outer copper layers. The toroid turns in Fig. 5a make a radial traverse around the core layer, so that the principal flux path lies in the FR4 core. In this arrangement, outer copper layers can both shield the device from stray capacitance and tap the toroid in a distributed manner. The inner vias were packed in a three-layer pattern comprising an inner dodecagon, squares, and equilateral triangles, all with edge lengths equal to a minimum via-trace-via spacing [8]. For a process with blind vias, one might embed the toroid completely within the PCB — as in Fig. 5b — provided the winding and distributed-capacitor designs can be effectively optimized in such an arrangement. To decouple the toroid and capacitive-tap design, we built some structures (shown in Fig. 6e and f) in which capacitors extended away from the magnetic structure: these tap areas could be scaled roughly independently of the capacitance per unit length along the winding.

The measured impedance of a PCB solenoid, with capacitor taps integrated into the board, is shown in Fig. 9. The mask layup for this structure is depicted in Fig. 6b. Four inductances and three capacitance values for this structure were computed by Cauer synthesis, yielding 3 even-harmonic impedance nulls and for an 82 MHz fundamental. Section inductances were approximated by varying the width of Niwa's rectangular

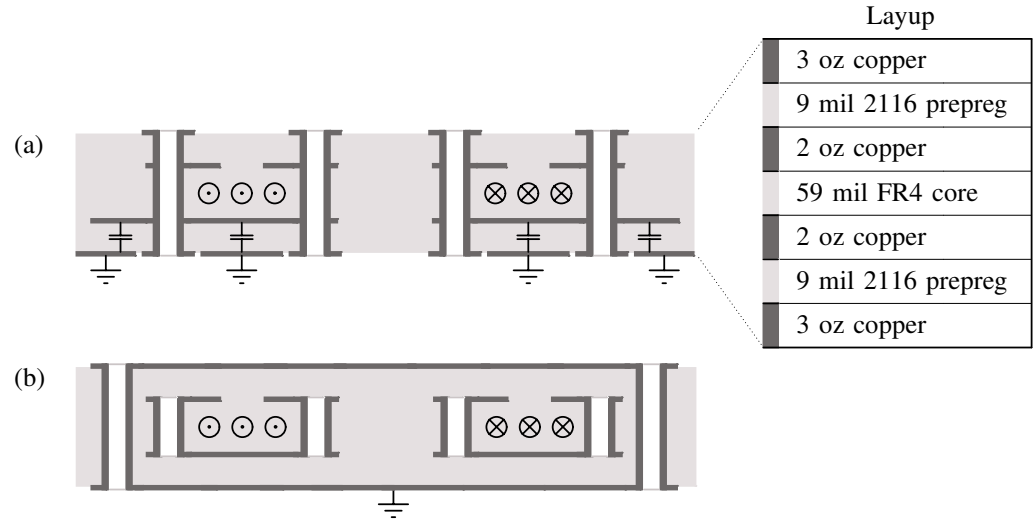

Fig. 5. **(a) Cross-sectional view and layup for a 4-layer PCB used to manufacture the tapped-inductor structures of Fig. 6. The board in (b) incorporates blind vias for more complete shielding of the embedded air-core magnetics.**

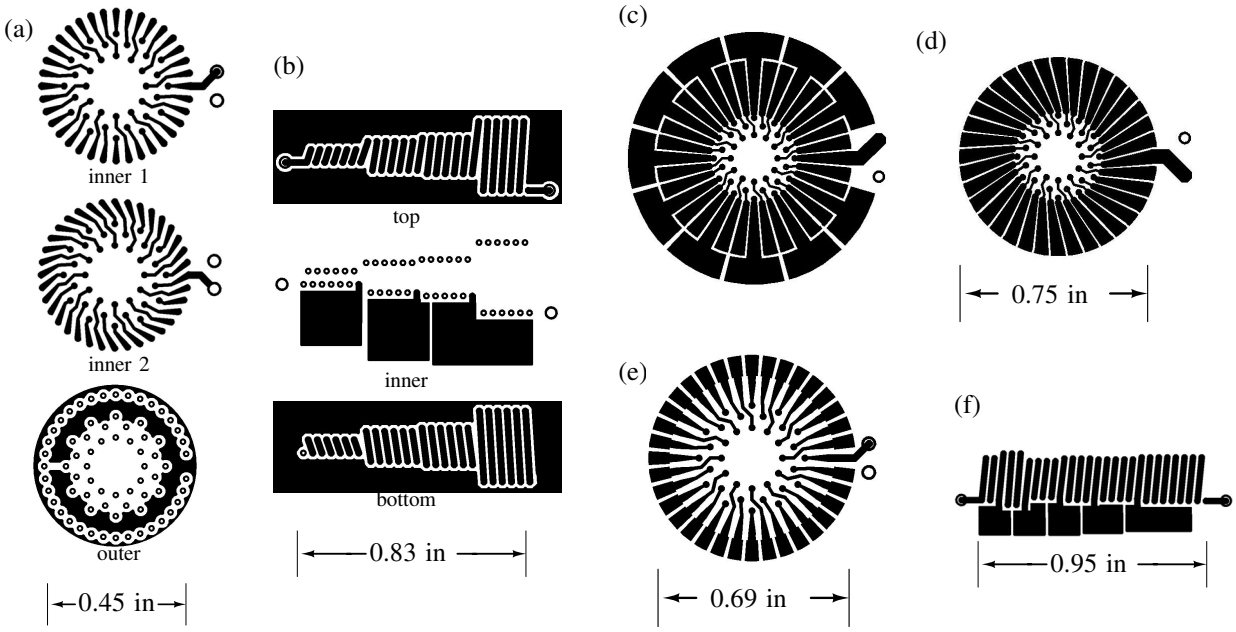

Fig. 6. **(a) and (b) show in-plane cross-sections for a shielded, toroidal inductor (a), and unshielded solenoid (b). The solenoid was designed by the Cauer-synthesis method described in the Appendix, and replaced the input class-E inductor L_{in} in the converter of Fig. 11a. (c) and (d) depict a 2-layer toroid with discrete capacitor taps, the measured impedance of which is shown in Fig. 3b. (e) a four-layer PCB toroid with 35 taps. Section inductances (Cauer-synthesis values) for (f) were approximated by varying the number of turns of Niwa's rectangular current-sheet approximation for solenoids with 0.2-inch width [6]. The width was then slightly adjusted to compensate for non-integral turns.**

current-sheet approximation for 6-turn solenoids[6]. The dc resistance of the completed structure was 62 mΩ.

B. Wafer-level Structures

A batch microfabrication process suitable for constructing multi-resonant magnetic structures on the surface of integrated circuits or other substrates was also developed. The toroids of Fig. 8 were constructed additively by electroformation, i.e., toroid turns were electroplated into a thick-film epoxy stencil. Our process centers around Microchem's SU-8 2005, a negative-tone photosensitive epoxy. Near-UV exposure with low doses yields stencil patterns with nearly vertical sidewalls and aspect ratios exceeding 15[9]. SU-8 2005 is a low-viscosity epoxy formulation designed for spin-application of 5-8 μm-thick films, though more viscous members of Michrochem's SU-8 family can coat up to 450 μm in a single step. We abandoned thick-film spin application after extensive experimentation with SU-8 2150 and 2100 (Microchem's most viscous formulations). Bubbles and nonuniform epoxy thickness prevented posts in later steps from simultaneously plating level with tops of their molds: overlying films then failed to cover the resulting steps. Films of lower-viscosity SU-8 2005, however, showed excellent thickness-uniformity when *poured*, uniformity that was key to the making reliable electrical connections above the wafer plane.

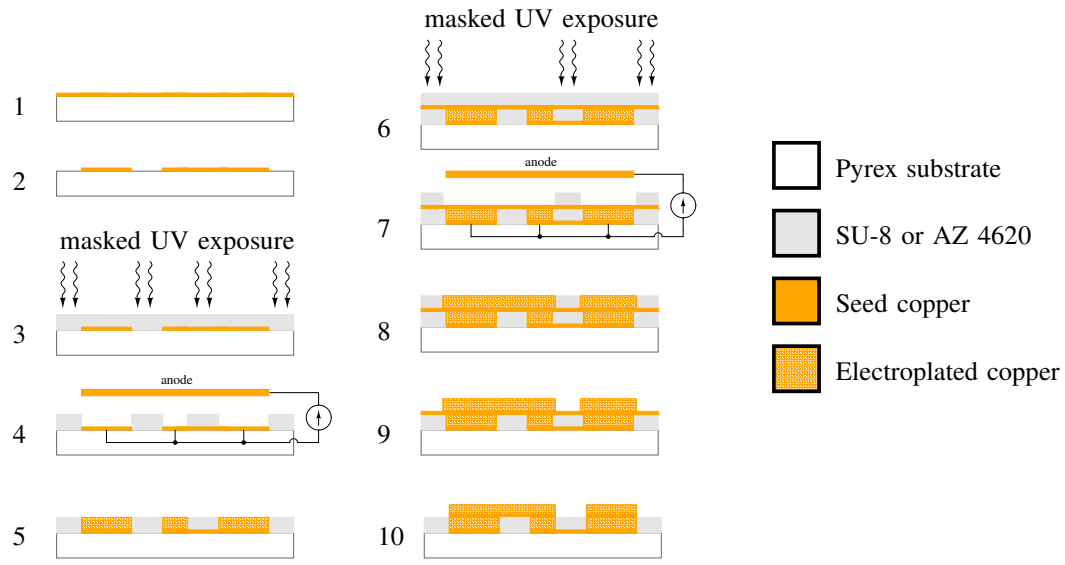

Fig. 7. **A MIcro-Molding and Electroplating (MIME) process suitable for fabricating multi-layer, air-core magnetic structures. In the 2-layer process shown here, SU-8 stencils with 500 μm builds act as a mold for electroformed copper in step 4. 10 μm AZ 4620 is the electroforming resist for step 7.**

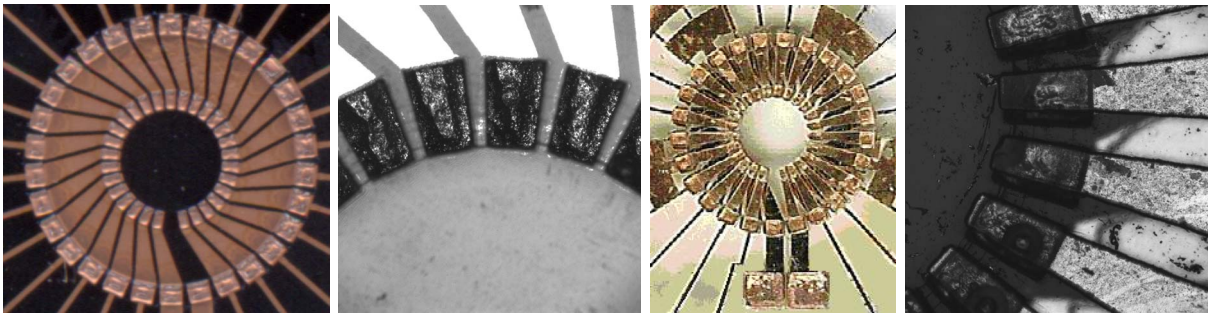

Fig. 8. **Die view (a) and detail of inner posts (b) of a 500 μm-thick electroformed toroid during step 5 in Fig. 7. A completed toroidal structure is shown in (c) and (d), with a detailed view of the top-level seed connecting to the top of an electroformed post.**

The process flow is outlined in Fig. 7. A bottommost 4000 Å Ti-Cu-Ti seed layer is evaporated Fig. 7-1, patterned Fig. 7-2, and electroplated to 20 μm thickness. The seed layer structures (cf. the staggered radial traces in Fig. 8a) connect turns of the overlying magnetic structure, and plate up in exposed regions to form high-build copper posts in the subsequent layer. Plating interconnects extend radially from this lowest metal layer, and extend to die boundaries so that dicing isolates regions shorted during electroformation. For the toroids shown in Fig. 8, a 500 μm film of SU-8 2005 was dispensed by pipette over the lower seed and confined to the wafer by a removable teflon mold. The epoxy film was then pre-baked on a scrupulously leveled hotplate for 16 hours, with a 2° C/hour ramp and hold from 65 to 95° C. This rising temperature and long prebake was necessary to uniformly drive solvent out of the film, a film that was — in the case of our thickest successfully developed application of 1.2 mm — 200 times thicker than the spin-coated thickness. The SU-8 is exposed (Fig. 7-3) with contrast-enhancement lithography using a topcoat Shin-Etsu CEM-388SS, and developed to clear inner and outer rings of wells. The achievable density of features in SU-8 indicates that 50-60 turn toroids are feasible in half-millimeter builds with the footprint shown in Fig. 8. SU-8 wells (the dark rectangles in the photos of Fig. 8b, see Fig. 7-5) mold copper in the first, high-build electroformation step.

After e-beam deposition of a second 4000 Å Ti-Cu-Ti seed, crossbars are electroformed in a lower-build, 10 μm mold of AZ 4620. Unlike SU-8 — which is notoriously resistant to solvents, acids and bases — hard-baked AZ 4620 is readily removed in acetone (Fig. 7-9). A slow etch-back step in 0.5 M sodium persulfate then clears unplated seed regions in several minutes, leaving plated copper dimensions nearly unchanged. Such a plate and etch-back step was necessary to improve metal step coverage over well edges: the AZ 4620 was never required, as an etch resist would, to cover steps to protect an underlying metal.

The measured impedance magnitude of best-performing plated toroid, tapped with three 15 pF mica capacitors, is shown in Fig. 10. The structure had a 10 MHz Q of 9.8 and an inductance of 48 nH at the same frequency. Poor contacts in the top metal layer to the tops of electroformed posts are responsible for the low Q, which can be greatly improved

by higher-build, strippable electroforming resists (i.e., higher copper build) in the top layer.

V. Applications

In this section we describe some of the applications of multi-resonant inductors and transformers, and highlight the benefits they can provide. We also introduce a new RF power amplifier topology that incorporates a multi-resonant inductor, and experimentally demonstrate the component and performance enhancements that the multi-resonant inductor provides.

As described in the Appendix, two-terminal lossless networks can be classified by their impedance characteristics at $s = 0$ and $s = \infty$, as determined by their finite, non-zero critical frequencies (alternating poles and zeros) along the $j\omega$ axis. Two types of network start with a zero at $s = 0$ frequency (a dc short) and differ in whether they have a pole or zero at $s = \infty$. The other two networks have a pole at the origin (a dc open) and again differ by whether they have a pole or zero at $s = \infty$. These behaviors at limiting frequencies can be convenient depending on the manner in which harmonic relations of poles and/or zeros are utilized. Below we consider both single-port networks, designed to provide a useful impedance across two terminals, and multi-port transformer networks, in which the self and mutual impedances of the ports are of interest.

A. Resonant Impedance Generation

Multi-resonant networks can be employed to generate impedance characteristics that are useful in many switching power converter applications. Consider, for example, a two-terminal multi-resonant structure having a zero at dc and a pole at $s = \infty$, with poles at some fundamental frequency its first several harmonics (zeros in such a case are perforce interspersed between the harmonics). Such a network would act as a short circuit at dc and an open circuit to periodic ac waveforms having the specified fundamental frequency. It is a higher-order version of the resonant network of Fig. 2a, able to present much higher impedance to periodic ac waveforms of the specified fundamental than could be achieved by a comparable inductor. Such a network could replace an inductor in a wide range of switching power applications, including any direct converter, as exemplified in Fig. 2a.

A similar resonant increase in impedance can be applied to transformers. Consider a transformer in which the primary and secondary windings are tightly magnetically coupled, and in which capacitive tapping of the primary and/or secondary yields a open-circuit primary-side impedance with pole-zero structure described above. The transformer's magnetizing impedance will now appear to be greatly increased for any periodic drive waveform of the appropriate fundamental frequency. Such a network is a multi-resonant version of the tuned transformer circuit of Fig 2c.[2] It could replace a conventional transformer in many power applications where the drive waveforms are periodic, and could extend the cases in which a transformer with a core may be replaced by a coreless multi-resonant design [5]. A transformer with similar impedance maxima — but with a zero at $s = 0$ — could also be useful in many inverter applications. Such a dc-blocking transformer, as described in Section III moreover, is readily implemented in iterated form.

B. Symmetry Relations

Multi-resonant magnetic structures can also impose desirable symmetries in converter waveforms. Any periodic waveform $x(t)$ of period T that possesses only fundamental and odd-harmonic content exhibits half-wave symmetry: $x(t) = -x(t - T)$ for all t. I.e., if the waveform has some value at a certain time, it will have the negative of that value a half-cycle later (or more generally, a value symmetric about the waveform's dc level). Such half-wave symmetries can be employed to great effect in many power electronics applications.

We can impose half-wave symmetry in converter waveforms through proper structuring of the poles and zeros of multi-resonant networks. Consider a multi-resonant inductor with impedance zeros at dc and even multiples of some fundamental frequency, and poles at the fundamental and odd harmonics. In this case, the tapped inductor acts as an open circuit to half-wave symmetric waveforms, and a short circuit to all even-harmonics components. Such an impedance is quite useful, especially as it may be easily realized by an iterated network as described in Section III. To elaborate further, if a circuit periodically imposes a certain voltage waveform on such a multi-resonant inductor during one half of the period, the network (in periodic steady state) will become energized so as to impose half-wave symmetry during the other half of the period.[3]

The multi-resonant components described find ready application in single-ended power converters. Consider the Class E inverter of Fig. 11a, for the design of which see [10], [11]. The input choke inductor L_{in} is sized to provide an approximately constant current into the converter, and is typically the largest passive component in the circuit. Here we introduce a new power amplifier, illustrated in Fig. 11b, in which the input choke inductor is replaced with a multi-resonant network having the impedance characteristics described above (i.e., zeros at even-harmonic multiples of the inverter operating frequency). Consider the steady-state operation of this new circuit for a switch duty cycle of slightly lower than 50%: The switch imposes a constant voltage (V_{in}) across the multi-resonant inductor during the first portion of the switching cycle (when the switch is on). When the switch turns off, the multiresonant inductor acts to drive the drain voltage up to $2V_{\text{in}}$ for an equal time period, and then back down to zero (for half-wave symmetry of the multi-resonant-network voltage). At this point, the switch may be turned on with zero-voltage switching, and the cycle repeats.

[2] As with the circuit of Fig. 2c, the resonant currents internal to the transformer and capacitors generate the bulk of the magnetizing flux.

[3] This property is analogous to the manner in which an inductor becomes energized such that it imposes zero average voltage across itself during periodic-steady-state operation.

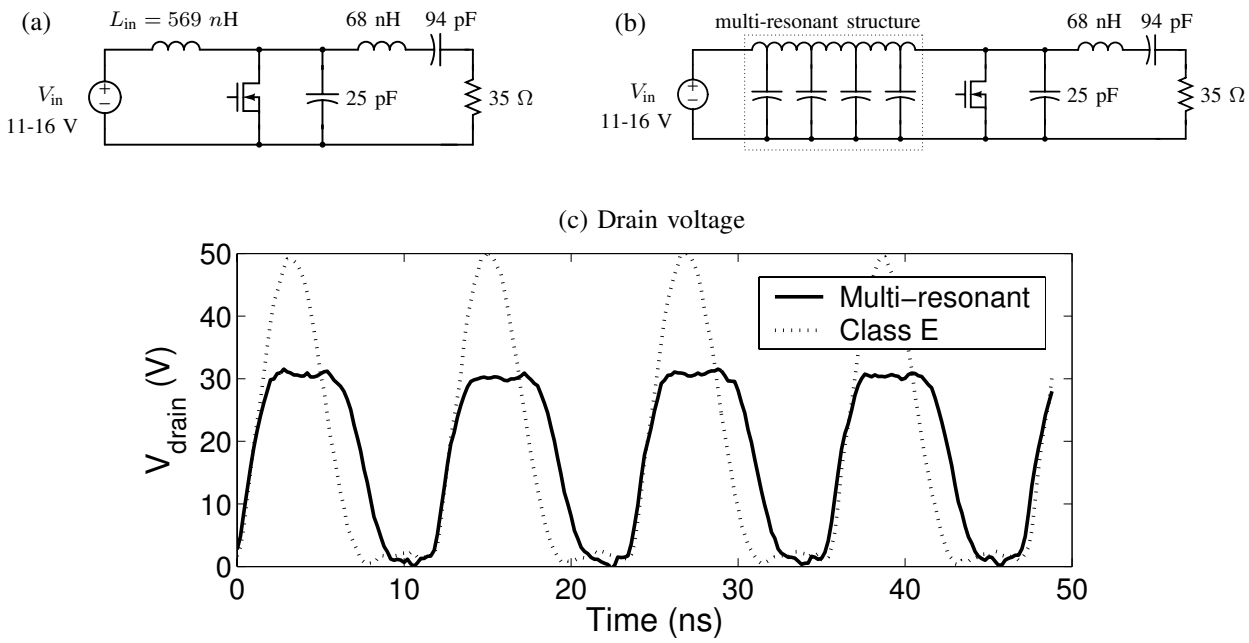

Fig. 11. **Comparison of drain-voltage waveforms for a 82 MHz class-E inverter (a) and an inverter in which input inductor L_{in} has been replaced by the multi-resonant PCB structure of Fig. 6b. The impedance of this structure is shown in Fig. 9. An STMicroelectronics PD57018 65 V FET was used in both converters, though the lower drain voltage in the multi-resonant case is compatible with a lower-voltage switch.**

This new power amplifier has significant advantages over the conventional class-E design. Peak transistor voltage in this new power amplifier is significantly reduced as compared to an equivalent Class E converter (cf, Fig. 11c, measured for V_{in}=16 V). Furthermore, the multi-resonant inductor can be made significantly smaller than the conventional inductor of the class E. In the constructed system of Figs. 11a and b, for instance, an L_{in} of 569 nH was replaced by a tapped PCB inductor of 238 nH (the 4-layer structure, cross-sections of which are shown in Fig. 6b). Inductance reduction of 5 to 6 times is possible with better alignment of impedance peaks and nulls (notice the mediocre alignment of the tapped structure, the impedance-magnitude plot for which is shown in Fig. 9). Greater size reduction — indeed, lower peak drain voltages, higher efficiency, and greater power — should be realizable when parasitics of our fabrication methods are better characterized. Both inverters maintained soft-switching at 82 Mhz: the broader, approximately square-wave drain voltage (31 V peak) of the multi-resonant inverter delivered 1.49 A p-p into the 13.5 Ω load through the $Q = 10$ output filter; the class-E design, for 50 V peak drain voltage, delivered 1.98 A p-p into the same load. The lower switch stress in the multi-resonant case would allow the 65 V PD57018 FET of the class-E inverter to be replaced with a 40 V member of the same family, the PD55025, with an $R_{ds,on}$ 2.7 times smaller than the higher-voltage FET. The efficiency of both inverters was between 80 and 84%, without considering gate-drive losses. For practical details and measurements of such high-frequency converters — self-exciting resonant gate drives, rectifier loads, regulation strategies, and methods of maintaining 75% total efficiency across load — refer to [12].

Multi-resonant transformers may also impose half-wave symmetry on their waveforms. Consider, for example, the push-pull converter of Fig. 12a, in which two switches are used to generate a square-wave ac output on the transformer secondary. Replacing the center-tapped transformer with a multi-resonant transformer having the appropriate dynamics allows the second switch and primary winding to be eliminated, as suggested by Fig. 12b.

C. Other Applications

Many other power applications can also benefit from appropriately designed magnetic structures. For example, Class F power amplifiers often use Foster reactance networks (e.g., with impedance peaks at odd harmonics of a fundamental) to reduce the voltage stress on the semiconductor as compared to a Class-E Amplifier ([13] Chapter 15). An integrated multi-resonant network allows the desired impedance characteristic to be implemented in a single structure (see Appendix for a discussion of such volume reduction).

APPENDIX

Though iterated L/C sections provide a close approximation to transmission-line impedances, more detailed synthesis methods use non-uniform L and C to place zeros and poles at specified frequencies. Before treating the problem of synthesis, consider an exemplary reactance function $X(s)$ to be synthesized, with a finite number of poles at $s = 0$, $\pm s_2$, $\pm s_4$, ... $s = \infty$ and zeros at the points $s = \pm s_1$, $\pm s_3$, $\pm s_5$, ...

$$X(s) = G \cdot \frac{(s^2 - {s_1}^2)(s^2 - {s_3}^2)(s^2 - {s_5}^2)\cdots}{s(s^2 - {s_2}^2)(s^2 - {s_4}^2)(s^2 - {s_6}^2)\cdots} \qquad (6)$$

This development starts with an even-over-odd reactance function, and hence a pole at the origin. A zero at $s = 0$ would shift the conventional indices of critical frequencies — the

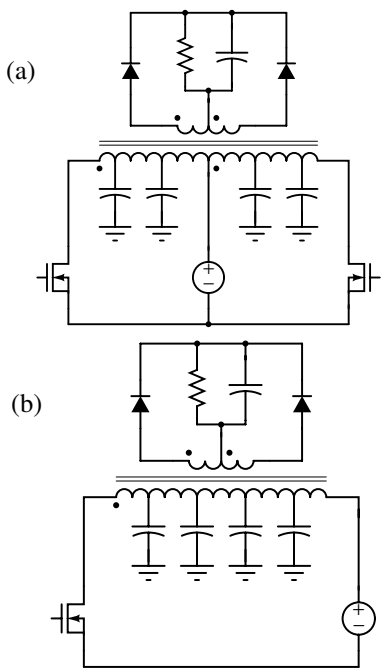

Fig. 12. **(a) A voltage-fed push-pull converter, illustrating an application of multi-resonant networks. (b) Waveform symmetry imposed by a multi-resonant magnetizing impedance allows a primary winding and one switch to be eliminated. Note that the rectifier load is not necessary for application of a multi-resonant network: rf amplifiers, for instance, could also benefit from higher magnetizing impedance.**

pole and zero frequencies, numbered in increasing order with $0 < \omega_1 < \omega_2 < \omega_3 < \omega_4 < ...$ — so that poles would have *odd-numbered* indices, and zeros *even-numbered*. The pole or zero at $s = \infty$ is determined by the relative degree of numerator and denominator in $X(s)$, and is independent of behavior at $s = 0$.[4]

$X(s)$ may be written in terms of the residues k_0, k_2, k_4, ... k_∞ of its poles at $s = 0$, $\pm j\omega_2$, $\pm j\omega_4$,... and $s = \infty$ respectively:

$$X(s) = \frac{k_0}{s} + \frac{2k_2 s}{s^2 + {\omega_2}^2} + \frac{2k_4 s}{s^2 + {\omega_4}^2} + ... + k_\infty s \qquad (7)$$

As may be verified in a small example with Heaviside's "cover-up" method of computing partial-fraction numerators (*viz.*, $k_n = [(s - s_\nu)X(s)]_{s=s_\nu}$), the residues may be determined from the slope of the susceptance function $B(s) = X(s)^{-1}$ [14]:

$$k_\nu = \left[\frac{dB(s)}{ds}\right]^{-1}_{s=s_\nu}$$

This interesting result provides a ready means of synthesizing a reactance (or susceptance) function when its zeros and slope are easily determined. Component values in the so-called series Foster form (Fig. 13a) can be determined by a term-by-term comparison of the Foster impedance Z_F to Eqn. 7:

$$Z_\mathrm{F} = \frac{1}{sC_0} + \frac{\frac{1}{C_2}s}{s^2 + \frac{1}{L_2 C_2}} + \frac{\frac{1}{C_4}s}{s^2 + \frac{1}{L_4 C_4}} + \cdots + \mathbf{Ł}_\infty$$

from which

$${\omega_\nu}^2 = \frac{1}{L_\nu C_\nu} \quad \text{and} \quad 2k_\nu = \frac{1}{C_\nu} \quad \text{for } \nu = 2, 4, 6, ...$$

and $C_0 = {k_0}^{-1}$ and $L_\infty = k_\infty$. Rewriting in terms of the susceptance slope:

$$C_\nu = \frac{1}{2}\left[\frac{dB(s)}{ds}\right]^{-1}_{s=s_\nu} \quad \text{and} \quad L_\nu = \frac{1}{C_\nu {\omega_\nu}^2}$$

for $\nu = 2, 4, 6, ...$. Referring back to the short-circuit admittance Y_sc of the transmission line in Eqn. 3, the zero admittance frequencies are[5]

$$\omega_\nu = \frac{\nu\pi}{2\ell\sqrt{LC}} \quad \text{for } \nu = 1, 3, 5, ...$$

[4]In fact, we do not need to specify a pole or zero at $s = 0$ or $s = \infty$ beyond enumeration of finite nonzero critical frequencies. The alternation property of poles and zeros requires poles at $s = 0$ and $s = \infty$, for instance, when the lowest and highest non-zero critical frequencies are zeros.

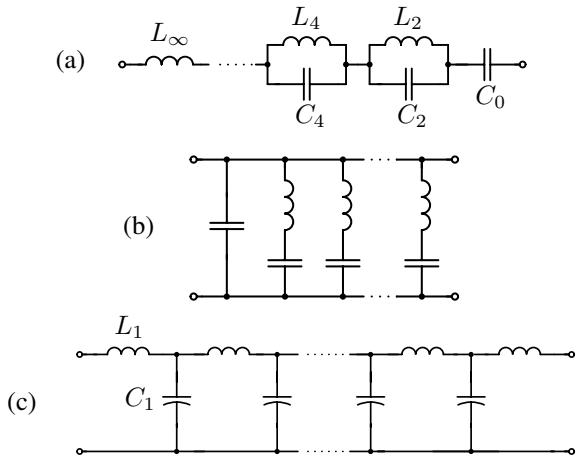

Fig. 13. **Canonical forms discussed in Appendix: (a) series Foster form, (b) parallel Foster form, and (c) Cauer form**

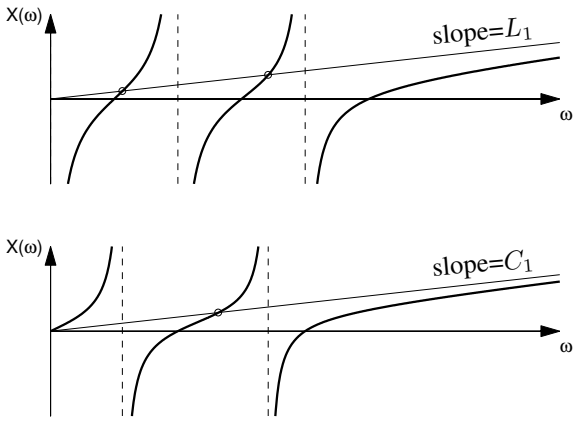

Fig. 14. **Illustration of two steps in the Cauer-synthesis procedure for the network in 13c. An inductive reactance ωL is subtracted, in the impedance domain, from the reactance to be synthesized. The zeros shift after this operation, to become the poles of a susceptance function, below.**

[5]Note that numbering of critical frequencies has shifted: zeros starting at $s = 0$ now alternate with *odd* numbered poles

from which the Foster capacitances can be found:

$$\left[\frac{dY_{\text{in}}^{\text{sc}}}{ds}\right]_{\omega=\omega_\nu} = \sqrt{\frac{C}{L}}\frac{\ell\sqrt{LC}}{\sin^2\theta_\nu} = C\ell = C_{\text{tot}} \qquad (8)$$

I.e., $C_\nu = C_{\text{tot}}/2$, where C_{tot} is the total line capacitance. The corresponding modal inductances L_ν decrease as the square of the mode-number:

$$L_\nu = \frac{8L_{\text{tot}}}{\nu^2\pi^2} \quad \text{where} \quad L_{\text{tot}} = L\ell \qquad (9)$$

I.e., the characteristic impedance and coupling of higher-order resonances — for a finite, lumped transmission-line analog — decrease with frequency.

For the parallel Foster form (Fig. 13b), a dual development from a partial-fraction expansion for susceptance is straightforward:

$$L_\nu = \frac{1}{2}\left[\frac{dX(s)}{ds}\right]^{-1}_{s=s_\nu} \quad \text{and} \quad C_\nu = \frac{1}{L_\nu{\omega_\nu}^2}$$

for $\nu = 1, 3, 5, ...$, in which $s_\nu = j\omega_\nu$ are the poles of $Y(s)$ and the zeros of $Z(s)$. In the transmission-line case, again noting a shift in the numbering of critical frequencies, the derivative of $Z_{\text{in}}^{\text{sc}}$ (Eqn. 1) yields series-tuned inductances and capacitances:

$$L_\nu = \frac{L_{\text{tot}}}{2} \qquad C_\nu = \frac{8C_{\text{tot}}}{\nu^2\pi^2}$$

The Foster forms are volume-inefficient realizations of transmission-line impedance characteristics beyond two or three resonances: they require, for each peak or null, one component which is half as large as the corresponding total-line value (L_{tot} or C_{tot}). A so-called Cauer form, such as that shown in Fig. 13c, is particularly volume-efficient, on the other hand, because modal inductances and capacitances arise from different modeshapes on the *same structure*. The Cauer-network model — to a degree that improves with the number of discrete sections — is made up of iterated T- or L-section models of incremental portions of line.

Cauer-network values approximate the incremental L and C of the modelled line for very large numbers of sections, but may be found by a method of residue removal for a realizable number of sections. A desired reactance or susceptance function is first written in factored form, as shown in Eqn. 6 (for a power-converter application with switching frequency f_{sw}, one might choose nulls at $s = 0$ and all even multiples of f_{sw}, with poles at odd multiples of f_{sw}). Residues at $s = \infty$ are successively substracted in the reactance or susceptance domains, corresponding to the removal of the component which dominates — at very high frequencies — the impedance of the network to be synthesized. For the Cauer form of Fig. 13c, for instance, the high-frequency impedance seen from either port is dominated by the end-section inductors: the adjacent capacitors are effectively short-circuits.

Removal of a residue at $s = \infty$ is illustrated graphically in Fig. 14. The zeros of the reactance function shift as the line with slope sL_1 is subtracted from $X(s)$ (i.e., as the series inductor is removed from network). In the susceptance domain, the process begins again, with the subtracted admittance sC_1 corresponding to a removed terminal capacitance. By successively working along a network with poles and zeros at transmission-line frequencies, the last residues are found to increase in the last steps of the synthesis procedure (cf. the horn-like solenoid structures of Fig. 5, where inductance and capacitance increase toward the right). Recall that in the Foster realization of the transmission-line impedance, either modal capacitance or modal inductance decreased as the mode-number ν squared. The total value of these tapering values roughly equals the total corresponding value in the Cauer network, taking account of the increase of values toward the end of the synthesis procedure. The total *constant* modal L or C in the Foster form ($C_{\text{tot}}/2$ or $L_{\text{tot}}/2$), however, is much larger than the corresponding Cauer value beyond two or three modelled resonances.

ACKNOWLEDGMENTS

The authors wish to thank the United States Office of Naval Research for support of this research under ONR grant N000140010381

REFERENCES

[1] J. Phinney, *Filters with Active Tuning for Power Applications*. S.M. thesis, Dept. of Electrical Engineering and Comp. Science, Massachusetts Institute of Technology, Laboratory for Electromagnetic and Electronic Systems, 2001.

[2] J. Phinney and D. Perreault, "Filters with active tuning for power electronics," *IEEE Power Electronics Specialists Conference*, pp. 363–370, June 2001.

[3] J. Phinney and D. Perreault, "Filters with active tuning for power electronics," *IEEE Trans. Power Electron.*, vol. 18, pp. 636–647, March 2003.

[4] R. Balog and P. Krein, "Automatic tuning of coupled inductor filters," *IEEE Power Electronics Specialists Conference*, vol. 2, pp. 591 –596, June 2002.

[5] S. Tang, S. Hui, and H.-H. Chung, "Coreless planar printed-circuit-board (PCB) transformers — a fundamental concept for signal and energy transfer," *IEEE Transactions on Power Electronics*, vol. 15, pp. 931–941, September 2000.

[6] F. Grover, *Inductance Calculations*. New York: Dover, 1946.

[7] T. Neugebauer and D. Perreault, "Filters with inductance cancellation using printed circuit board transformers," *IEEE Trans. Power Electron.*, vol. 19, May 2004.

[8] P. Murgatroyd, "The optimal form of coreless inductors," *IEEE Transactions on Magnetics*, vol. 25, pp. 2670–2677, May 1989.

[9] R. Ruhman, K. Pfeiffer, M. Falenski, F. Reuther, R. Engelke, and G. Gruetzner, "SU-8 — a high-performance material for MEMS applications," *MSTnews*, vol. 41, pp. 45–46, January 2002.

[10] N. Sokal and A. Sokal, "Class E — a new class of high-efficiency tuned single-ended switching power amplifiers," *IEEE Journal of Sold-State Circuits*, vol. SC-10, pp. 168–176, June 1975.

[11] N. Sokal, "Class-E RF power amplifiers," *QEX*, pp. 9–20, Jan/Feb 2001.

[12] J. Rivas, R. Wahby, J. Shafran, and D. Perreault, "New architectures for radio-frequency dc/dc power conversion," in *35^{th} Annual Power Electronics Specialists Conference Proceedings*, June 2004.

[13] T. Lee, *Design of CMOS Radio-Frequency Integrated Circuits*. Cambridge, United Kingdom: Cambridge University Press, 1998.

[14] E. Guillemin, *Synthesis of passive networks: theory of methods appropriate to the realization and approximation problems*. New York: John Wiley & Sons, 1957.